Baroclinic Rossby Waves in a Square Basin*

J. H. LACASCE

Woods Hole Oceanographic Institution, Woods Hole, Massachusetts

(Manuscript received 20 July 1999, in final form 22 February 2000)

ABSTRACT

The properties of forced baroclinic, quasigeostrophic Rossby waves in an ocean basin are discussed, with emphasis on the apparent phase speed. The response to a traveling wave wind stress curl consists of three parts, two of which propagate westward and one that tracks the wind. The apparent phase speed in the basin interior depends on the relative sizes of the amplitudes of these three terms, which vary with forcing frequency and scale and with the size of the deformation radius. With low-frequency, large-scale forcing, one westward wave dominates and its phase speed is the long baroclinic Rossby wave speed. With smaller forcing scales, the component that tracks the wind is comparably strong, and the superposition with the dominant westward wave can produce augmented apparent phase speeds. At frequencies larger than the maximum free wave frequency (proportional to the deformation radius), the westward waves are trapped in deformation-scale boundary layers, yielding a weak, directly forced interior. The choice of boundary conditions is found to affect strongly the response. In contrast to wind forcing, forcing by an imposed boundary oscillation yields propagation at the long-wave speed over a wide range of forcing frequencies.

1. Introduction

The recent satellite altimeter observations of westward phase propagation by Chelton and Schlax (1996) have rekindled interest in oceanic Rossby waves. Besides demonstrating that a clear wave signal exists, the authors noted discrepancies between the apparent phase speed and the classical value predicted for a free baroclinic Rossby wave over a flat bottom. In particular, while the observed phase speed agreed approximately with theory in the Tropics, it was too fast in the subtropics. In a more recent analysis in which altimeter data from the North Pacific were sorted by wavenumber and frequency, Zang and Wunsch (1999) found that much of the observed energy propagates at the long-wave speed, but that discrepancies do exist at smaller horizontal scales.

These augmented phase speeds have received substantial attention. One explanation, advanced by White (1977) prior to the altimeter observations, is that the presence of an eastern boundary demands a free wave component to balance the directly forced response and that the superposition of the free and forced waves produces apparent phase speeds in excess of the long-wave speed (section 3).

Others have proposed alternate explanations. Qiu et al. (1997) suggest that lateral (eddy) diffusion can make waves appear faster by changing their east–west structure. Killworth et al. (1997) and Dewar (1998) show how a mean baroclinic shear can alter baroclinic wave speeds, and Dewar (1998) and de Szoeke and Chelton (1999) explore the effects of subsurface, homogeneous potential vorticity (PV). Topography could also play a role, for instance by causing the waves to become surface-trapped and hence faster (e.g., Rhines 1970; Samelson 1992). Or the effect may simply be a statistical one, related to forcing at a multitude of frequencies and spatial scales (K. Brink 2000, personal communication).

In other words, there are numerous possible explanations. Interestingly, most of these studies concern free Rossby waves, or forced waves in a semi-infinite ocean. Of course the Pacific and Atlantic are of finite width, so it makes sense to revisit the problem of forced waves in a basin. The purpose of the present work is to do so, and to examine the apparent phase speeds along the way. Perhaps surprisingly, the simple system considered here exhibits features common with the observations of both Chelton and Schlax (1996) and Zang and Wunsch (1999).

Forced Rossby waves in a basin were first considered by Pedlosky (1965), who examined the barotropic, quasigeostrophic case. That solution comprises three wave terms, one that tracks the wind and two westward waves required to satisfy the boundary conditions in the east

* Woods Hole Oceanographic Institution Contribution Number 10029.

Corresponding author address: Joe LaCasce, Woods Hole Oceanographic Institution, M.S. 29, Woods Hole, MA 02543.
E-mail: jlacasce@whoi.edu

and west. The spatial extent of each term depends strongly on forcing frequency, and not all three are necessarily present in the interior at a given frequency (see below).

The present work is essentially the baroclinic version of Pedlosky's: a square, quasigeostrophic ocean with one moving layer above a resting lower layer, with a traveling-wave-type wind forcing. The dependence on forcing frequency, dissipation, deformation radius, and forcing scale will be considered, and the solution compared to that obtained with the frequently used long-wave equation, like that of White (1977). Waves forced by boundary oscillations will also be considered, and contrasted with wind-driven waves.

2. Wind-forced solutions

The linear, quasigeostrophic potential vorticity equation for a moving upper layer above a motionless lower layer is

$$\frac{\partial}{\partial t}(\psi_{xx} + \psi_{yy} - 1/\lambda^2\psi) + \beta\psi_x = \frac{\nabla \times \tau}{\rho_0 H} - r(\psi_{xx} + \psi_{yy} - 1/\lambda^2\psi), \qquad (1)$$

with ψ the velocity streamfunction ($\mathbf{u} = \mathbf{k} \times \nabla\psi$), λ the deformation radius, $\beta = \partial f/\partial y = \text{const}$, τ the wind stress, and H the depth of the layer (e.g., Pedlosky 1987). The last is a linear damping term that simulates the dissipation of PV (chosen among other possibilities for mathematical simplicity). In the limit $\lambda \to \infty$, we recover the barotropic equation considered by Pedlosky (1965).

Following Pedlosky (1965), Eq. (1) can be nondimensionalized with the following substitutions:

$$(x, y) = L(x', y'), \qquad t = (\beta L)^{-1}t',$$

$$\nabla \times \tau = \frac{\tau_0}{L}F, \qquad \psi = \frac{\tau_0}{\rho_0\beta H}\psi',$$

where L is the width of the basin. Then the nondimensional PV equation (dropping primes) is

$$\frac{\partial}{\partial t}(\psi_{xx} + \psi_{yy} - 1/\lambda^2\psi) + \psi_x = F - r(\psi_{xx} + \psi_{yy} - 1/\lambda^2\psi), \qquad (2)$$

where r has been replaced by $r/(\beta L)$, and λ by λ/L. The forcing will be taken to be a propagating, monochromatic wind stress curl; that is, $F = \cos(kx - \omega t)$.

Parameter values

Before discussing solutions to (2), it is worthwhile mentioning to what dimensional values the dimensionless parameters correspond. For a basin like the Pacific, the deformation radius is much smaller than the basin width, so λ is a small number. A typical value assumed hereafter is $\lambda = 0.01$, although in the Pacific it is even smaller. Given the smallness of λ, a more appropriate set of equations might be the planetary geostrophic equations (e.g., Charney and Flierl 1981), which permit order one interfacial deviations. However, the quasigeostrophic equations are a useful starting point; future work would necessarily permit such higher-order dynamics.

With a basin 10 000 km wide and a value of $\beta \approx 2 \times 10^{-11}$ (ms)$^{-1}$, a frequency of roughly 0.001 corresponds to a period of one year. It is not certain how large r ought to be, that is, how fast PV is dissipated, so various values will be considered. But a value of $r = 1.5 \times 10^{-4}$ corresponds to a damping time of one year with these parameters.

3. The long-wave solution

Before examining the full two-dimensional basin solution, it is instructive to consider the solution to (2) with no y variation. Without forcing or boundaries, the solution is composed of the free Rossby waves generated by the initial condition. These possess the well-known dispersion relation (e.g., Gill 1982):

$$\omega = -\frac{k}{k^2 + 1/\lambda^2}. \qquad (3)$$

From this, one may deduce that the maximum wave frequency is $|\omega| = \lambda/2$, which occurs at $k = 1/\lambda$. Large scales are associated with low frequencies, and in the long-wave limit ($k \ll 1/\lambda$), the phase speed approaches a constant, $c = \omega/k \approx -\lambda^2$, hereafter the "long-wave phase speed."[1]

If the scales of motion are much larger than the deformation radius, one may neglect the relative vorticity in (2) and obtain a first-order wave equation. White (1977) derived the solution to this equation under the condition $\psi = 0$ at $x = 1$ (the eastern boundary) for the special case of no zonal wind variation ($k = 0$). Retaining zonal variability, the solution (valid in the region $-\infty < x < 1$) is found to be

$$\psi = \text{Re}\left\{\frac{\lambda^2}{-r + i(\omega + k\lambda^2)} \times \left[-\exp\left(\frac{(r - i\omega)(x - 1)}{\lambda^2} - i\omega t + ik\right) + \exp(ikx - i\omega t)\right]\right\}, \qquad (4)$$

where Re{ } indicates the real part. Solution (4) has two

[1] Note this is the long-wave phase speed in one and a half layers. As such, the phase speed is greater than the baroclinic Rossby wave speed in two layers over a flat bottom (e.g., Samelson 1992).

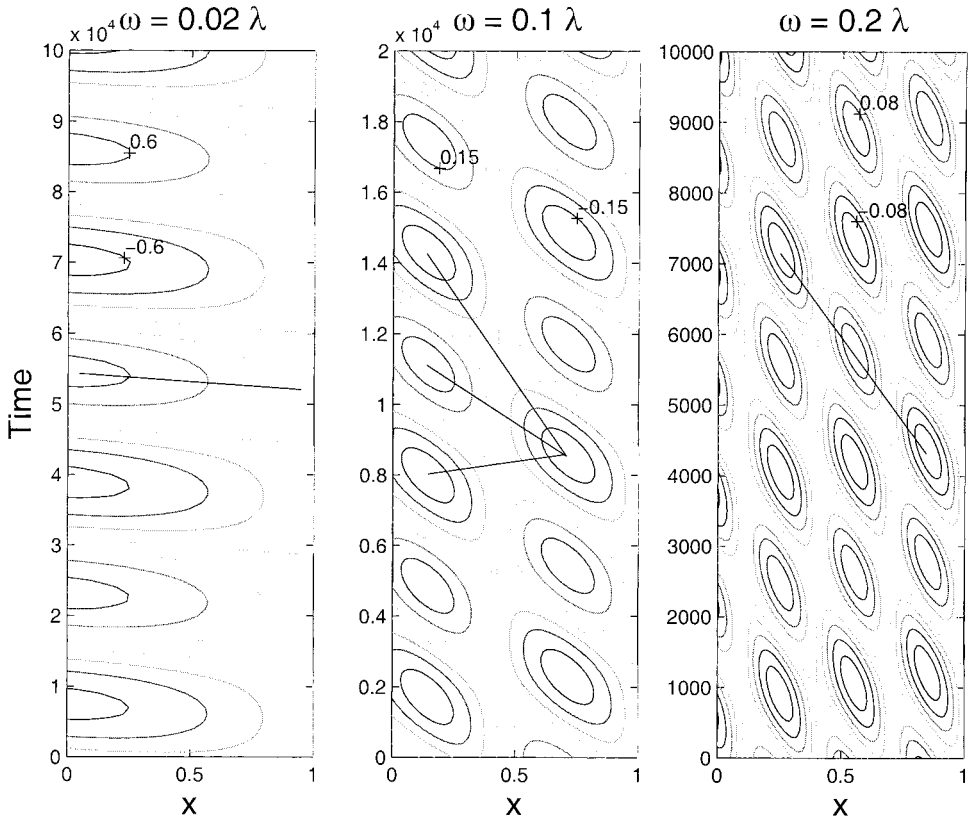

FIG. 1. Time–longitude plots from the first-order wave equation solution. The parameters are $k = 1$, $\lambda = 0.01$, and $r = 0$. The augmented phase speed, derived in the text, is indicated by the solid lines; the values are $c = -4\lambda^2$, $c = -2.22\lambda^2$, and $c = -2.11\lambda^2$. In addition, the long-wave speed $c = -\lambda^2$ (upper line) and the wind phase speed $c = \omega$ (lower line) are indicated in the middle panel. The contour values are (left panel) $\pm$[0.2.4.6], (middle) $\pm$[0.05.1.15], and (right) $\pm$[0.02.04.06.08]. The corresponding dimensional frequencies for a Pacific-sized basin are approximately 5 yr; 1 yr, and 6 months. Note the y axis spans $20/(2\pi)$ forcing periods in each case.

constituents: a directly forced wave and a westward propagating wave required to satisfy the eastern boundary condition. The two are equal in amplitude (due to the boundary condition) and their combination possesses an apparent phase velocity faster than the long-wave speed. This can be seen by rewriting the inviscid version of (4), thus

$$\psi = \frac{2\lambda^2}{(\omega + k\lambda^2)} \sin\left(\frac{\omega + k\lambda^2}{2\lambda^2}x - \phi_3\right) \times \cos\left(\frac{\omega - k\lambda^2}{2\lambda^2}x + \omega t - \phi_3\right), \quad (5)$$

where $\phi_3 = \omega/(2\lambda^2) + k/2$ is a phase. Solution (5) consists of a traveling wave modulated by a stationary envelope function (the group velocity is zero). The phase velocity of the former is

$$c_l \equiv \frac{-2\omega\lambda^2}{\omega - k\lambda^2}. \quad (6)$$

This has an interesting frequency dependence. In the low-frequency limit ($\omega \ll \lambda^2$), c_l is twice the forcing phase speed, ω/k. At high frequencies, it approaches twice the long-wave speed, that is, $c \to -2\lambda^2$. It equals twice the long-wave speed at all frequencies when the forcing wavenumber, k, is zero, which is the special case of White (1977). At intermediate frequencies with $k \neq 0$ the phase speed is even greater.

Solution (4) can be used to construct time–longitude plots, and examples for various forcing frequencies are shown in Fig. (1). For the solution shown, $r = 0$, $\lambda = 0.01$, and the wind's zonal wavenumber was 1 (the results with $k = 0$ are similar).

The solid lines in the left and right sections and the middle line in the center panel indicate the augmented phase speed, c_l, from (6), and these lines are consistent with the observed tilt in the crests. The values of c_l for these cases are $-4\lambda^2$, $-2.22\lambda^2$, and $-2.11\lambda^2$, respectively. As shown in the center section, the long-wave speed and the wind phase speed $c = \omega/k$ can also be found by connecting different crests, and the augmented speed is seen to lie between the two.

Significantly, the total wave amplitude decreases

monotonically with increasing frequency. This stems from the inverse dependence on frequency of the wave amplitude in (5). Also of interest is the increase in small-scale structure with increasing frequency, which is due to the westward wave in (4).

4. 1D basin solution

Now we consider the basin solution without variation in y. Retaining relative vorticity, the solution validity is no longer restricted to large scales or low frequencies. Now there are two unknowns, which are determined by implementing the boundary conditions at the eastern and western walls.

However, one has to be careful about these boundary conditions. The streamfunction must be constant along the boundaries to prohibit normal flow there and, assuming a connected basin, it has the same value on the eastern and western walls.[2] But simply demanding $\psi = 0$ (as in section 3) yields a solution that does not conserve mass (McWilliams 1977; Flierl 1977; Milliff and McWilliams 1994). To remedy this, the boundary value is allowed to be an unknown function of time; that is,

$$\psi_{\text{boundary}} = \Gamma(t) = \gamma \exp(-i\omega t), \tag{7}$$

and γ is found by invoking the conservation of mass:

$$\frac{\partial}{\partial t}\int_0^1 \int_0^1 \psi \, dx \, dy = 0. \tag{8}$$

Physically, this boundary condition permits the interface to move up and down, rather than being ''pinned'' there. Allowing interfacial motion and invoking the conservation of mass significantly alters the forced response, as will be seen.

The solution to (2) with forcing, $F = \cos(kx - \omega t)$, is found to be

$$\psi = \text{Re}\left\{\left(\gamma - \frac{e^{ik}}{N}\right)\frac{\sinh(Ax)}{\sinh(A)}\exp(-\alpha(x-1) - i\omega t) - \left(\gamma - \frac{1}{N}\right)\frac{\sinh(A(x-1))}{\sinh(A)}\exp(-\alpha x - i\omega t) + \frac{1}{N}\exp(ikx - i\omega t)\right\}, \tag{9}$$

where the constants are

$$\alpha \equiv \frac{1}{2(r - i\omega)} \qquad A \equiv \frac{(1 + 4((r - i\omega)/\lambda)^2)^{1/2}}{2(r - i\omega)}$$

$$N \equiv ik - (k^2 + 1/\lambda^2)(r - i\omega).$$

[2] This assumption is strictly speaking inconsistent, without northern and southern boundaries. Nevertheless, the solution will be shown to resemble the 2D solution with forcing of large meridional extent; see section 6.

With no y variation, the mass conservation condition (8) is simply a zonal integral from west to east. Solving for γ, one finds

$$\gamma = \frac{B_a e^{ik} - B_b - \left(\frac{1}{ik}\right)\sinh(A)(e^{ik} - 1)}{N(B_a - B_b)}, \tag{10}$$

where the two additional constants are

$$B_a = \frac{1}{2}\left[\frac{e^A - e^{-\alpha}}{-\alpha + A} - \frac{e^{-A} - e^{\alpha}}{-\alpha - A}\right]$$

$$B_b = \frac{1}{2}\left[\frac{e^{-\alpha} - e^{-A}}{-\alpha + A} - \frac{e^{-\alpha} - e^{A}}{-\alpha - A}\right].$$

Despite the plethora of constants, solution (9) is relatively simple in form. It is composed of three wave terms: the first two have westward phase speeds and are required to satisfy the boundary conditions in the east and west, and the third has the same phase speed as the wind. The apparent phase speed for the full solution depends on the relative sizes and phase speeds of these three terms.

In the absence of forcing ($F = 0$), the solution involves the basin modes excited by the initial condition. Under the rigid interface approximation ($\Gamma = 0$), the basin-mode frequencies are determined by the condition $A = in\pi$, for which $\sinh(A)$ vanishes (e.g., Pedlosky 1965). Without damping, these frequencies are given by

$$\omega = \frac{1}{2[n^2\pi^2 + 1/\lambda^2]^{1/2}}. \tag{11}$$

With $\Gamma \neq 0$, these frequencies are no longer resonant; one can show that the two westward waves cancel one another when $\sinh(A) = 0$, leaving only the (finite) directly forced wave. However, the denominator in (10) can vanish when $B_a = B_b$, or equivalently when $\cosh(\alpha) = \cosh(A)$. This yields a slightly different set of resonant frequencies:

$$\omega = \frac{2m\pi}{(4m^2\pi^2 + 1/\lambda^2)}. \tag{12}$$

Interestingly, these new frequencies are exactly those of free baroclinic waves with an integral number of wavelengths in the basin (the physical reason for this is discussed in section 5). In the barotropic limit ($\lambda \to \infty$) the resonant frequencies are identical to those in (11), but for smaller values of λ they are subtly, but significantly, different (Fig. 2). While the high frequency cutoff is $\lambda/2$ in both cases, the cutoff occurs at $n = 0$ in (11) whereas in (12) it occurs at $m = 1/(2\pi\lambda)$. The frequency decreases monotonically with increasing mode number in (11), but in (12) the frequency *increases* from zero to $\lambda/2$ for $m < 1/(2\pi\lambda)$ and decreases thereafter. Thus the resonance mode number is not a single-valued function of the frequency when $\Gamma \neq 0$.

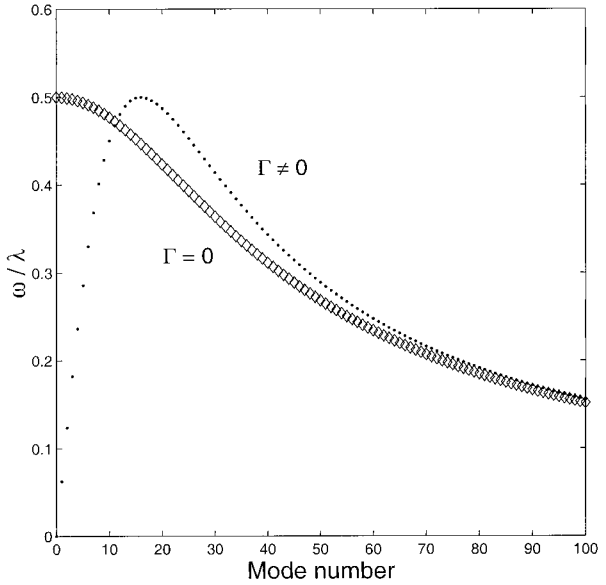

FIG. 2. Resonance frequencies vs mode number for the 1D basin solution with $\lambda = 0.01$, with the rigid interface boundary condition ($\Gamma = 0$) and with $\Gamma \neq 0$.

Unlike with $\Gamma = 0$, low-frequency driving can produce resonances of large scale, and changing the forcing frequency only slightly can excite a mode of very different scale.

a. Frequency and dissipation

To understand solution (9), it helps to look at two limiting cases: the low forcing frequency and dissipation limit, and the high-frequency limit. Consider the former. Assuming $\omega \ll \lambda$ and $r \leq \omega$, we have

$$A \approx \alpha + (r - i\omega)/\lambda^2.$$

Away from the boundaries, solution (9) can be rewritten:

$$\psi \approx (\gamma e^{ik} - 1/N)\exp\left(-\frac{r(1-x)}{\lambda^2} - \frac{i\omega(x-1)}{\lambda^2} - i\omega t\right) + (\gamma - 1/N)\exp\left(-\frac{rx}{s^2} - \frac{i\omega x}{s^2} - i\omega t\right) + (1/N)\exp(ikx - i\omega t), \quad (13)$$

where $s^2 \equiv r^2 + \omega^2$. The first term in (13) has a phase speed equal to the long-wave speed, $c = -\lambda^2$, and a zonal wavelength, $\propto \lambda^2/\omega$, which increases with decreasing frequency; hereafter, this will be referred to as the ''long-wave'' component. The long wave decreases in strength moving westward from the eastern boundary so long as there is dissipation. Note that the corresponding wave term in the full solution (9) actually vanishes at the western wall, yielding small-scale structure not captured by (13).

The second term (to be called the ''short-wave'') has a slower phase speed, $c = -s^2 \approx -\omega^2$ and a shorter zonal wavelength, $\propto s^2/\omega \approx \omega$. With dissipation, the short wave decreases in strength moving eastward from the western boundary. This term should be compared to the short Rossby wave generated upon reflection of a long wave at a western boundary (Pedlosky 1987).

The phase speed of the third wave term is that of the wind, $c = \omega/k$. This term will be referred to as the ''directly forced'' wave.

As mentioned, the two westward waves decay into the interior, one from each boundary; however, the boundary layers are unequally wide. The western boundary has a width $\propto s^2/r \approx \omega^2/r$ and the eastern a width $\propto \lambda^2/r$. By assumption, $s^2 \ll \lambda^2$, so the eastern layer is much thicker. The reason for the difference is related to the different group velocities; from (3), we have

$$c_{gx} = \frac{k^2 - 1/\lambda^2}{(k^2 + 1/\lambda^2)^2}. \quad (14)$$

Plugging in the expressions for the zonal wavenumbers from (13), we find the long wave has a westward group velocity and the short wave an eastward velocity, and that the magnitude of the former is much greater. For instance, if $\lambda = 0.01$ and $\omega = 0.1\lambda$, the long-wave group velocity is $c_{gx} = -0.971\lambda^2$ whereas the short wave has $c_{gx} \approx (\omega/\lambda)^2\lambda^2 = 0.01\lambda^2$. So the long wave can travel much farther during the damping e-folding timescale.

A qualitative change in A, and hence the solution, occurs when the forcing frequency exceeds the maximum free wave frequency. If $\omega > \lambda/2$, one has

$$\frac{\sinh(A(x-1))}{\sinh(A)} \to \exp\left(-\frac{x}{\lambda}\right) \quad \text{and}$$

$$\frac{\sinh(Ax)}{\sinh(A)} \to \exp\left(-\frac{1-x}{\lambda}\right)$$

so that both westward waves are trapped in deformation-scale boundary layers. The only term of importance in the interior then is the directly forced wave, and the apparent phase speed must equal the wind's. Boundary trapping at high frequencies occurs whether or not there is dissipation, unlike at low frequencies.

As mentioned above, the observed phase speed will depend on the relative sizes of the three wave terms in (9). This is somewhat difficult to assess a priori, given the form of γ, so we resort to calculating numerically the various terms.

Shown in Fig. 3 are the magnitudes of the three wave constituents at the basin center, $x = 0.5$, for two values of r (corresponding to damping times of 7.5 years, and 9 months). Consider the less dissipative case. At low frequencies ($\omega < 5 \times 10^{-4}$), the short wave is confined to the western wall, and only the long and directly forced waves are evident. These terms are of comparable amplitude at the lowest frequencies.

At intermediate frequencies ($5 \times 10^{-4} < \omega < \lambda/2$), resonances are apparent. Note the long wave may have

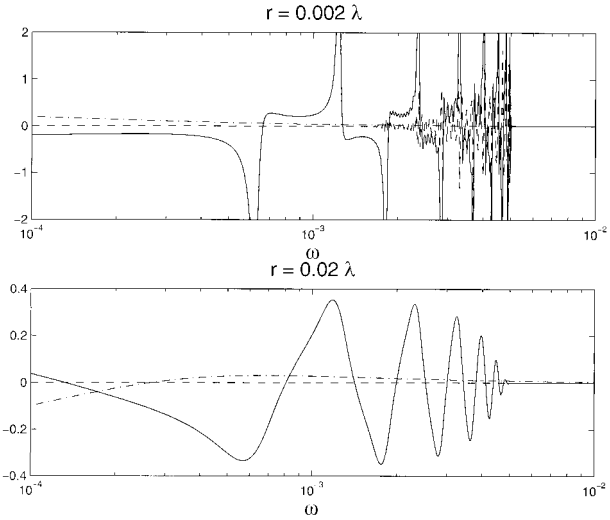

FIG. 3. The amplitudes of the three wave terms at the basin center as functions of frequency. The corresponding values of dissipation are as shown. The solid line is the long-wave term, the dashed is the short wave, and the dash–dot the directly forced wave. The high-frequency cutoff $\lambda/2$ is 0.005.

a large amplitude despite the lack of the short wave in the interior (contrary to what we would expect for the barotropic normal modes; see section 5). As $\omega \to \lambda/2$, the short wave appears in the interior. The directly forced wave is subdominant at most frequencies in this range.

In the high-frequency range ($\omega > \lambda/2$), only the directly forced wave is present in the interior, as both westward waves are confined to deformation-scale wall layers. Because the directly forced wave has an amplitude that decreases with increasing frequency, the interior response is correspondingly weaker.

With more dissipation (lower panel), the short wave is never observed in the interior. The long wave is still the strongest at frequencies less than $\lambda/2$, but weaker than with $r = 0.002\lambda$. The resonances, still evident, have been greatly smoothed out.

The above variations are mirrored in time–longitude plots constructed from (9). Four examples are shown in Fig. (4) for progressively higher frequencies. The dissipation has been set to $r = 2 \times 10^{-5} = 0.002\lambda$, corresponding to a damping time of 7.5 yr with the Pacific parameters.

With $\omega = 0.02\lambda$ (a period of 5 yr), the directly forced and long waves are comparably strong at the basin center (Fig. 3), while the short wave is confined to a thin layer in the west (and is not visible); as pointed out by Pedlosky (1965), the latter is essentially a time-dependent Stommel layer. The long wave decays from the eastern boundary, with a phase tilt consistent with the long-wave speed, whereas the directly forced wave has a tilt consistent with the wind speed and does not vary in amplitude across the basin. The two cancel in the basin center but not on the boundaries, and it is difficult to discern the sense of phase propagation.

But with $\omega = 0.1\lambda$ (a 1-yr period), the sense is clear because the long wave dominates. Here the long wave is as strong as at $\omega = 0.02\lambda$, but the directly forced wave is weaker and the short wave is still confined to the west. The phase speed is thus the long-wave speed (indicated by the solid line).

At $\omega = 0.2\lambda$ (half-year period), the short wave is evident in the interior, indicated by the small scale structure in the west. In the east the long wave is still the strongest, and its phase speed is evident. In fact, the speed is somewhat *slower* than the long-wave speed at this frequency [which is no longer small enough to justify expression (13)]. It can be shown that the phase speed lies between $c = -\lambda^2$ and $c = -\omega^2$; here it is only about 5% slower than the long-wave speed.

At $\omega = \lambda$ (1.2-month period), the westward waves are trapped at the western and eastern walls, and only the directly forced wave is found in the interior; thus the observed phase speed is eastward, like the wind's. As implied in Fig. 3, the amplitude in the interior is rather weak. However, the westward waves are as strong as at lower frequencies, though trapped at the boundaries. In other words, there is little variation in their amplitude with forcing frequency.

As noted before, changing the dissipation alters the widths of the layers in which the westward waves are trapped. As such, increasing the dissipation an order of magnitude to $r = 0.02\lambda$ with $\omega = 0.2\lambda$ causes the short wave to recede to the western wall (Fig. 5). Increasing it further to $r = 0.2\lambda$ confines the long wave to the eastern boundary. In contrast, both waves extend undiminished across the basin with no damping at all, because A is purely imaginary if $r = 0$ and $\omega < \lambda/2$ so that the sinh terms in (9) are purely sinusoidal.

b. Deformation radius

Increasing/decreasing the (nondimensional) deformation radius λ is like decreasing/increasing the forcing frequency, due to the dependence of A in (9) on $[(r - i\omega)/\lambda]^2$. Decreasing λ also lowers the maximum free wave frequency, which favors a high-frequency response like that described in the last section (with the westward waves trapped in deformation-scale boundary layers).

Shown in Fig. 6 are time–longitude plots for three values of λ with the annual period forcing ($\omega = 10^{-3}$) and a dissipation time of 7.5 yr ($r = 2 \times 10^{-5}$). With $\lambda = 0.01$, the response is the same as that at the same frequency in Fig. 4. Increasing λ to 0.1 yields a solution more like that at $\omega = 0.02\lambda$ in Fig. 4; the directly forced and long waves are comparably strong and cancel each other at the basin center (the small-scale structure near the eastern wall is actually due to the long wave; the short wave is not visible).

In the limit of large λ (the barotropic limit), $A \approx \alpha = 1/[2(r - i\omega)]$ and the solution is independent of the deformation radius. Incidentally, the difference between the solutions with $\psi = \Gamma$ and $\psi = 0$ on the boundary

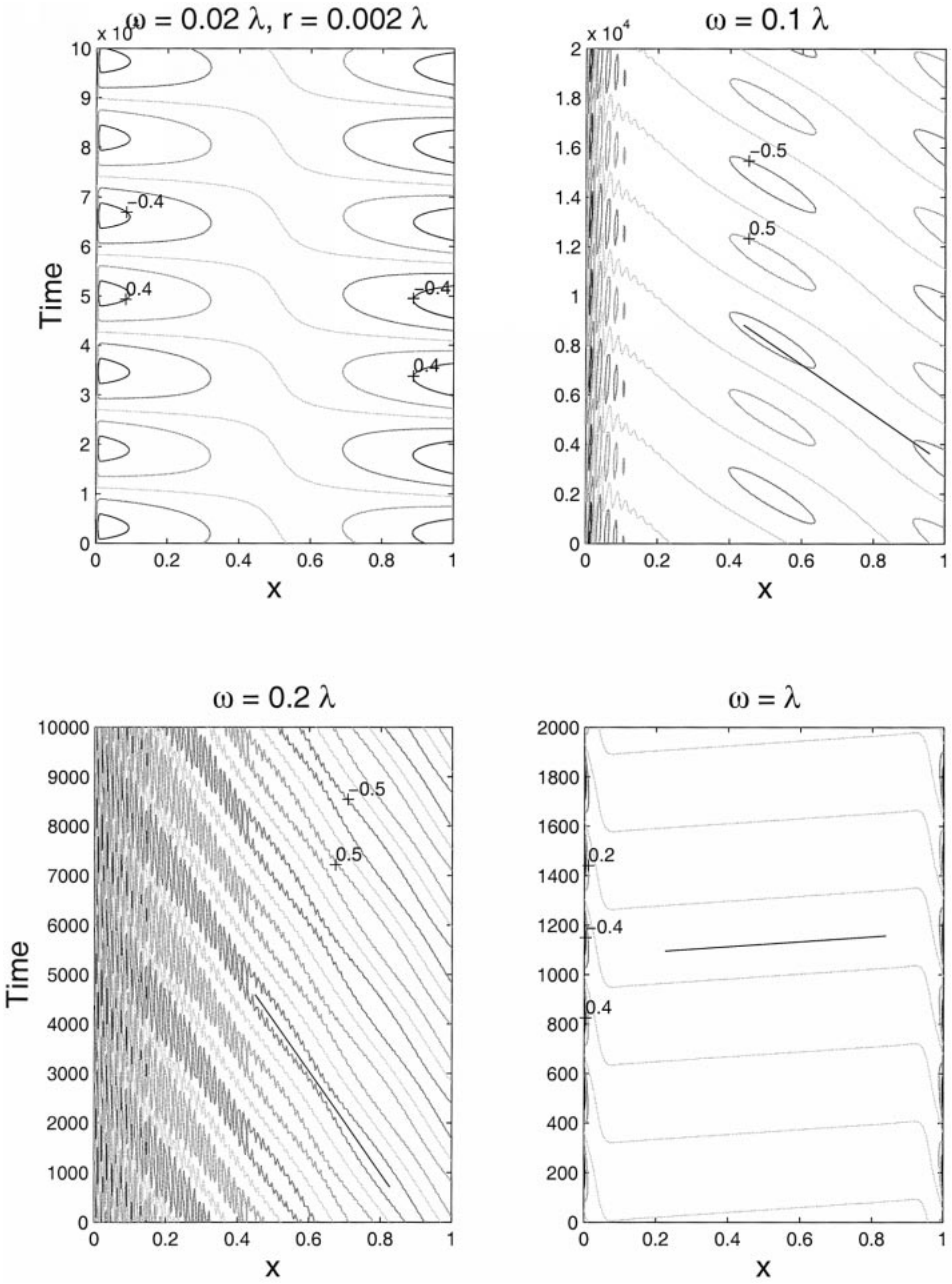

FIG. 4. Time–longitude plots of basin waves with no y variation, with $\lambda = 0.01$, $k = 1$, and $r = 2 \times 10^{-5}$. The solid line in the upper-right panel indicates the long-wave phase speed, and in the lower left panel a somewhat slower speed, $c = -0.95\lambda^2$. The line in the right panel indicates the wind phase speed, $c = \omega$. The contour values are (upper left and lower right) $\pm[0.2.4]$ and (upper right and lower left) $\pm[0.51]$.

vanish in this limit because mass is trivially conserved with a rigid lid (Flierl 1977).

As suggested above, decreasing λ makes it more likely the westward waves will be boundary trapped at a given forcing frequency; with $\lambda = 0.001$, the forcing frequency of 10^{-3} exceeds $\lambda/2$ and trapping is evident (right panel of Fig. 6). Note too that the boundary layers are smaller because the deformation radius itself is.

c. Zonal wavenumber

Because A is independent of k, changing the zonal wavenumber of the wind has no effect on the spatial distribution of the westward components. However, increasing k reduces the amplitudes of all the wave constituents, and the decrease is more marked for the westward waves than for the directly forced wave.

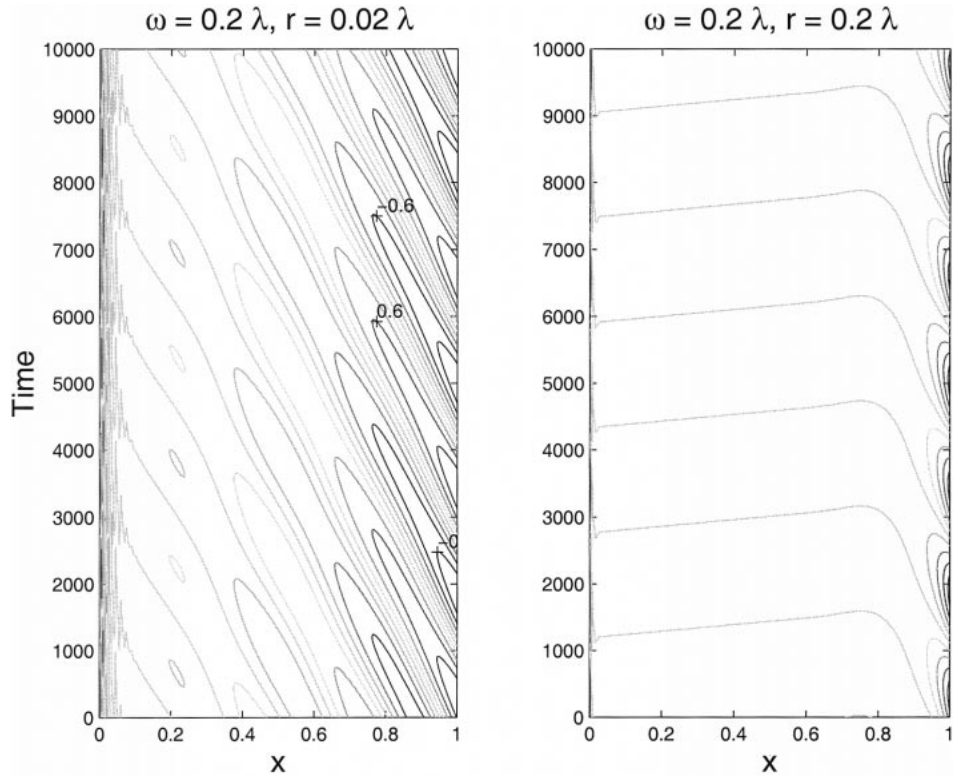

FIG. 5. The solution with $\omega = 0.2\lambda$ from the previous figure, but with more dissipation. The contour values are $\pm$[0.2.4.6.8]. Note the increased tendency for boundary trapping.

This is seen in Fig. 7. The parameters here are the same as in the upper right panel of Fig. 4. With $k = 0$, the solution is almost identical to that with $k = 1$ (Fig. 4). It is similar too with $k = 3$; although the long wave is somewhat weaker, it still dominates in the interior. However, with $k = 10$, the long wave is only as strong as the directly forced wave. (The patchwork appearance results because the long and directly forced waves have very different phase speeds, as indicated.) One observes clearly that the interior response weakens with increasing k.

In the limit that the wind scale is much less than the deformation radius ($k \gg 1/\lambda$), increasing k decreases the free wave frequency. Thus small forcing scales are like large forcing frequencies in that the westward waves do not extend into the interior.

5. Comparing the basin and long-wave solutions

The apparent phase speed for the basin solution thus spans a range of possible values. With large-scale forcing, the long-wave speed obtains at the lowest frequencies and the wind phase speed at the highest frequencies; for many intermediate values, the phase speed is approximately the long-wave speed. The long-wave solution (section 3) in contrast exhibits the wind phase speed at *low* frequencies, and twice the long-wave speed at larger frequencies. Why do the two solutions differ?

There are two possible causes: either the presence of the western wall or the alternate boundary condition used in the basin solution ($\Gamma \neq 0$). To see, consider the long-wave version of the basin solution calculated with $\Gamma = 0$. In the limit of weak dissipation and low forcing frequencies, this is

$$\psi \approx \frac{1}{k + \omega/\lambda^2}\left[-\exp\left(-\frac{r(1-x)}{\lambda^2}\right) \times \sin\left(-\frac{\omega(x-1)}{\lambda^2} - \omega t + k\right) + \exp\left(-\frac{rx}{s^2}\right)\sin\left(-\frac{\omega x}{s^2} - \omega t\right) + \sin(kx - \omega t)\right], \quad (15)$$

whereas the long-wave solution in the same limit is

$$\psi \approx \frac{1}{k + \omega/\lambda^2}\left[-\exp\left(-\frac{r(1-x)}{\lambda^2}\right) \times \sin\left(-\frac{\omega(x-1)}{\lambda^2} - \omega t + k\right) + \sin(kx - \omega t)\right]. \quad (16)$$

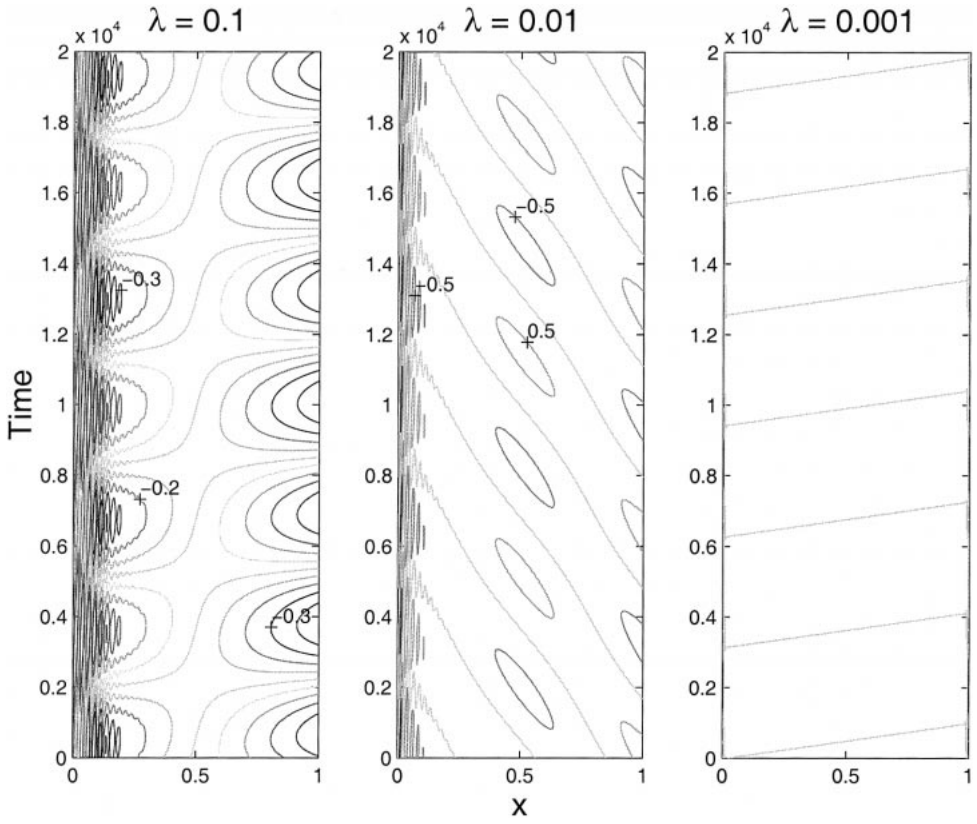

FIG. 6. The dependence on the ratio of the deformation to the basin scale. The forcing parameters are $\omega = 1 \times 10^{-3}$, $k = 1$, and $r = 2 \times 10^{-5}$, as in Fig. 4. Contour values are (left) $\pm$[0.1.2.3.4.5] and (middle and right) $\pm$[0.5].

These expressions differ only in the short-wave term in (15), which, as we have seen, only penetrates the basin interior at intermediate frequencies under weak dissipation; (15) and (16) are essentially identical at low frequencies in the interior.

The difference then stems from the boundary condition. Shown in Fig. 8 are the basin-wave amplitudes with the same parameters as those used in Fig. 3; the only difference is that $\psi = 0$ has been imposed at the boundary. Clearly the solution has changed greatly. The westward wave is always comparable in strength to the directly forced wave due to the imposed balance at the boundary, and all three waves weaken with increasing frequency. When the interface is permitted to move on the boundary, the westward waves can be much stronger than the directly forced wave and do not exhibit a systematic decrease with increasing frequency (Fig. 3).

Perhaps even more striking is the lack of resonances in Fig. 8. This, too, is related to the boundary condition. With $\psi = 0$ on the boundaries, a standing wave can be formed by the combination of two free waves, one associated with the eastern wall (with a westward group velocity) and a second with the western wall (with an eastward group velocity). These basin normal modes, with frequencies given in (11), are very susceptible to dissipation because of the slowness of the eastward Rossby group velocity.

With $\psi = \Gamma(t)$ on the boundary the situation changes because information can be transmitted from the western back to the eastern wall via the boundary oscillation, a process moreover which occurs instantaneously under the quasigeostrophic approximation (the Kelvin wave is infinitely fast). The eastward Rossby wave is no longer required, so the resonances are more robust to dissipation. But why are there resonances? With ψ equal at the eastern and western walls, the situation is very much like a periodic channel, as far as the waves are concerned; resonance occurs when the channel length is equal to an integral number of wavelengths, like acoustic waves in a clarinet, and hence the resonance condition in (12).

Of course these differences impact the observed phase speed. If the long wave and the directly forced wave have the same magnitude, their sum yields an augmented phase speed, as discussed in section (3), but if the long wave is much stronger than the directly forced wave, the long-wave speed will obtain.

6. 2D basin solution

Now we turn to the full two-dimensional solution to Eq. (1), obtained in the following manner. The inhomogeneous boundary condition, $\psi = \Gamma(t)$, can be converted to a homogeneous one by substituting $\psi = \phi + \Gamma(t)$ in (2). This results in a forcing term on the right-hand side of the transformed equation:

$$(r - i\omega)\frac{\gamma}{\lambda^2},$$

which is a constant at a given frequency. The equation can then be converted to an ODE in x, following a Fourier transform in time and a sine transform in y. The solution is found to be

$$\psi = \mathrm{Re}\left\{\sum_{n=1}^{\infty} \sin(n\pi y)\left[(H_2 - H_1 e^{ik})\frac{\sinh(A_n x)}{\sinh(A_n)}\exp[-\alpha(x-1) - i\omega t] - (H_2 - H_1)\frac{\sinh[A_n(x-1)]}{\sinh(A_n)}\exp(-\alpha x - i\omega t) + H_1\exp(ikx - i\omega t) - H_2\exp(-i\omega t)\right] + \gamma\exp(-i\omega t)\right\}, \tag{17}$$

where the constants are

$$\alpha \equiv \frac{1}{2(r - i\omega)}$$

$$A_n \equiv \frac{[1 + 4(r - i\omega)^2(n^2\pi^2 + 1/\lambda^2)]^{1/2}}{2(r - i\omega)}$$

$$H_1 \equiv \frac{f_n}{ik - (k^2 + n^2\pi^2 + 1/\lambda^2)(r - i\omega)}$$

$$H_2 \equiv \frac{2\gamma[1 - (-1)^n]}{n\pi(1 + n^2\pi^2\lambda^2)}.$$

I have assumed $F = \Sigma_n f_n \sin(n\pi y)\exp(ikx - i\omega t)$. The subsequent focus will be on the response to forcing at a single meridional wavenumber, denoted n_F, so that $f_n = \delta(n - n_F)$.

As before, γ is found by invoking conservation of mass, (8). The result can be shown to be

$$\gamma = -\left\{\sum_n \frac{[1-(-1)^n]}{n\pi} H_1\left[B_b - B_a e^{ik} + \frac{\sinh(A_n)}{ik}(e^{ik} - 1)\right]\right\} \Bigg/ \left\{\sum_n \frac{2[1-(-1)^n]^2}{n^2\pi^2(n^2\pi^2\lambda^2 + 1)}[B_b - B_a + n^2\pi^2\lambda^2\sinh(A_n)]\right\}, \tag{18}$$

where B_a and B_b are as in section 4, under the substitution $A \to A_n$. The solutions were evaluated numerically by summing truncated versions of the infinite series (approximately 500 terms).

Despite some added complexity, solution (17) has three propagating wave terms, each of which can be identified with one of the three terms in (9). Moreover, the extent to which the westward waves are boundary trapped as a function of frequency and dissipation is much the same because $A_n \approx A$ when $\lambda \ll 1$. The fourth term in (17) has an infinite phase speed, but is nearly cancelled by the boundary correction, $\gamma\exp(-i\omega t)$, in the limit $\lambda \ll 1$.

As discussed above, allowing $\psi \neq 0$ on the boundaries alters the resonant frequencies. The same is true in the 2D case; that is, the solution is finite in the inviscid limit when $\sinh(A_n) = 0$, and the resonances occur where the denominator of γ vanishes. However, the resonance condition is somewhat more complicated here because we require $B_b = B_a + n^2\pi^2\lambda^2$, which yields a transcendental equation for the frequencies. So the latter are best found numerically.

Likewise, it is also simpler to gauge the relative sizes of the wave constituents numerically. Several examples are shown in Fig. (9) for various values of n_F and with $\lambda = 0.01$ and $r = 0.01\lambda$ (a 1.5-yr damping time). The zonal wavenumber is zero here, and the plots show the wave amplitudes at $(x, y) = [\frac{1}{2},\ 1/(2n_F)]$ (this value of y corresponds to a peak in the sine expansion).

The constituent amplitudes with $n_F = 1$ are not greatly different than in the one-dimensional solution (Fig. 3; note r is different here). The long wave dominates at most frequencies, showing evidence of resonances, and only at the lowest frequencies is the directly forced wave comparably strong.

The result with $n_F = 2$ is quite different though; the long wave is much weaker, and comparable in strength to the directly forced wave. In fact, there is a strong

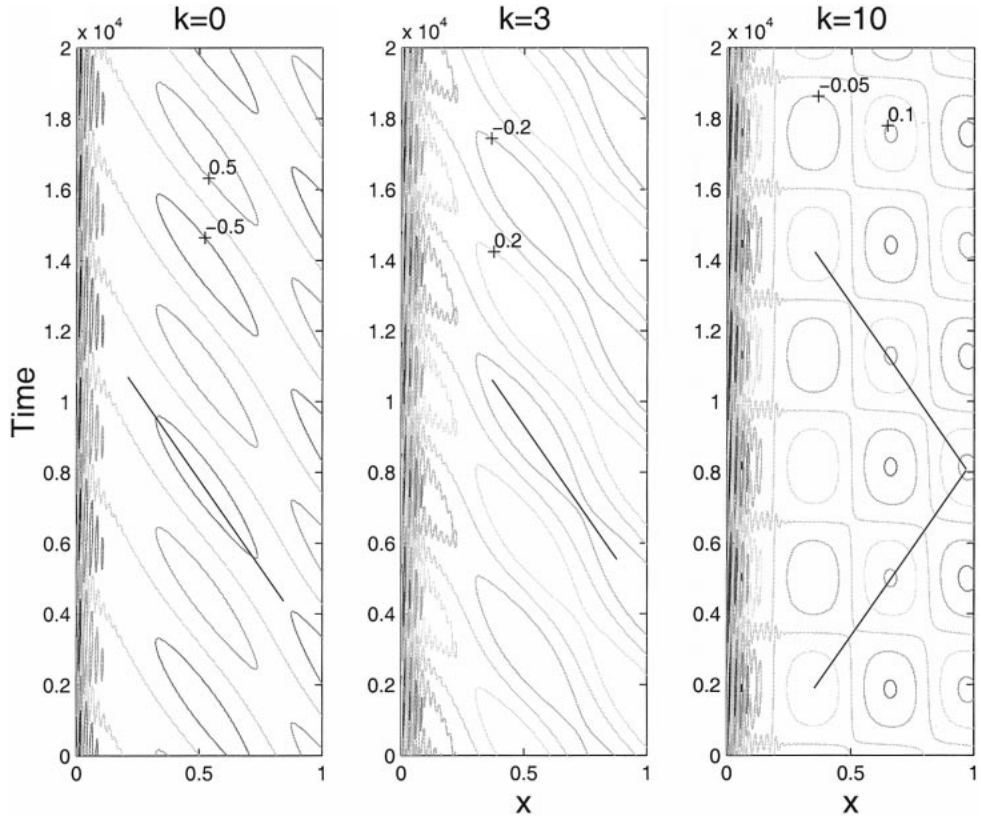

FIG. 7. The dependence on the zonal wavenumber of the wind. The forcing parameters are $\omega = 1 \times 10^{-3}$, $\lambda = 0.01$, and $r = 2 \times 10^{-5}$, as in Fig. 4. Solid lines indicated the long wave speed are shown as is one indicating the wind phase speed in the right panel. The contour values are (left) $\pm$[0.51], (middle) $\pm$[0.2.4.6], and (right) $\pm$[0.05.1.15].

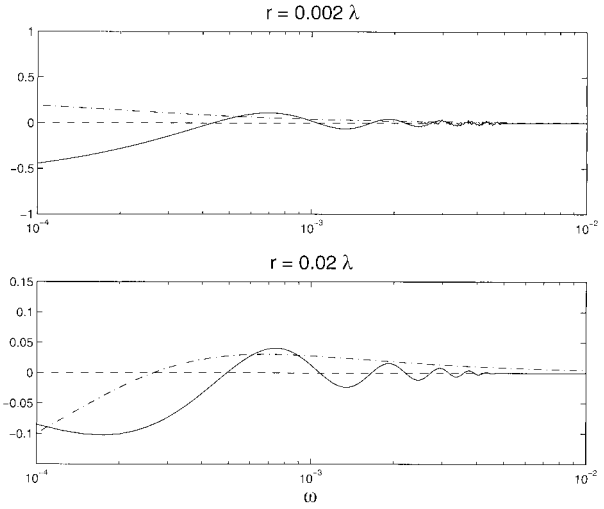

FIG. 8. The amplitudes of the three wave terms at the basin center with $\psi = 0$ taken on the boundaries. The parameters are as in Fig. 3.

resemblance to the case in which $\psi = 0$ was imposed at the boundary (Fig. 8). The reason is that γ in (18) is zero when n_F is even, that is, if the forcing is meridionally asymmetric about the center latitude.

The latter, somewhat nonintuitive result is related to the boundary condition under the QG approximation. As noted above, allowing $\psi = \Gamma(t)$ on the boundaries is like adding a forcing term that is constant at a given frequency, and the sine transform of a constant has the property that even mode number contributions (which have a node at the basin center) vanish. So the even modes vanish because $\Gamma(t)$ cannot vary in space, as required by QG. The same asymmetry was noted for the unforced modes by Flierl (1977). One suspects that the difference might not survive if the interface height could vary along the boundary, that is, if the QG approximation were relaxed.

Intuition suggests that large interfacial deflections will occur primarily for large-scale forcing, and that $\Gamma(t)$ will be smaller for smaller scales. This is the case; the solutions with $n_F = 5$ and 6 (lower panels) are much more alike, with a weaker long-wave contribution.

The total wave amplitude is noticeably weaker with larger n_F, and eventually the directly forced wave emerges as the dominant constituent (not shown). The

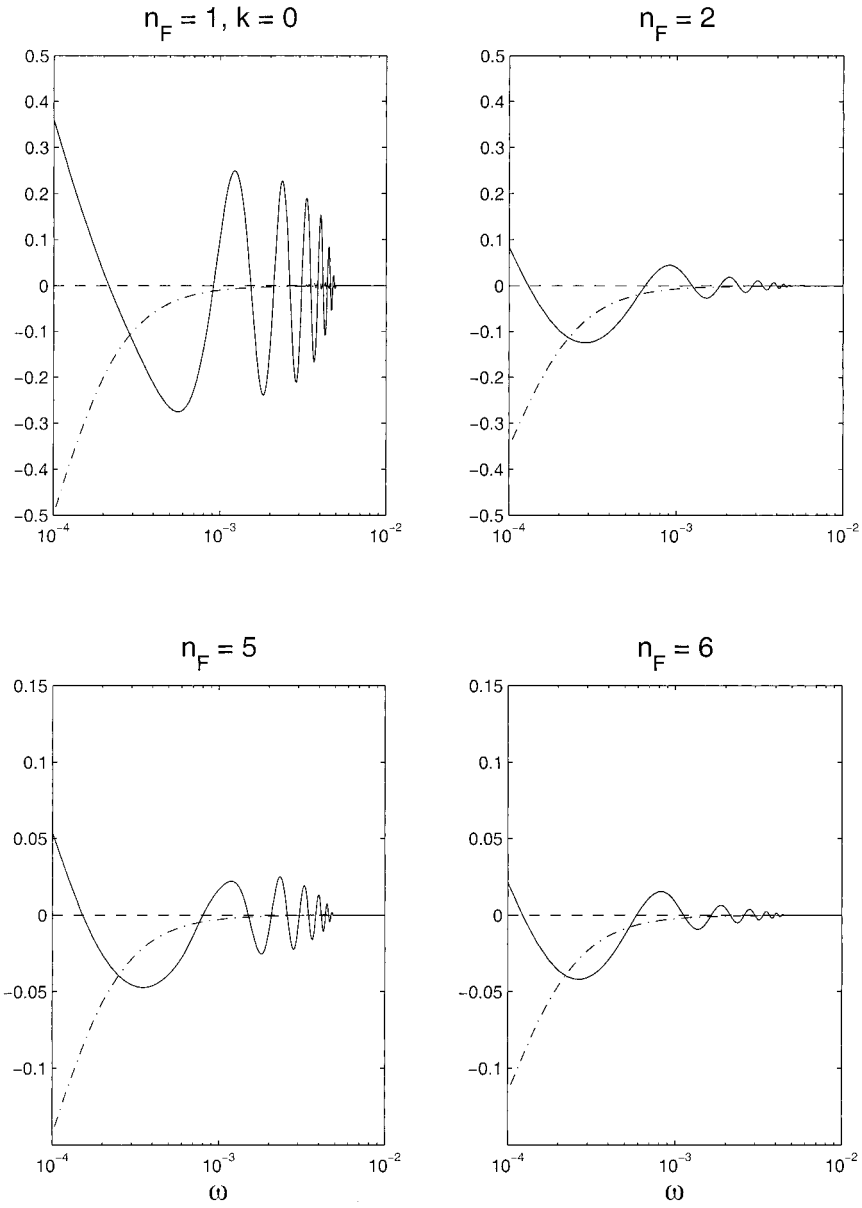

FIG. 9. The amplitudes of the three wave terms at $(x, y) = (\frac{1}{2}, 1/(2n_F))$ vs frequency from the 2D solution, with various meridional wavenumbers. The zonal wavenumber k is zero, $\lambda = 0.01$, and $r = 0.01\lambda$.

same is true for higher-zonal wavenumbers (k) at a fixed value of n_F, consistent with the one-dimensional results (section 4c). Recall that the wavenumber corresponding to the deformation radius in these examples is 100, so these transitions occur at much greater scales.

The variations with meridional wavenumber are even more striking in ''snapshots'' of the streamfunction, shown in Figs. (10) and (11). With $n_F = 1$, the streamfunction effectively spans the basin north to south, with boundary layers at each end and at the western wall (the general lack of meridional variation outside boundary layers is why the solution with $n_F = 1$ resembles the 1D solution of section 4). The response with $n_F = 2$ is much different, having a more regular, drumlike modal appearance and a smaller amplitude.

The solution with $n_F = 3$ (upper panel of Fig. 11) displays a sizeable minimum in the middle of the eastern basin and boundary layers to the north and south. The minimum moves westward, and evolves into a two-lobed feature as it passes the basin center (the remains of the previous maxima are still evident). It then continues westward, with its aspect continuously evolving. In contrast, the solution with $\psi = 0$ on the boundaries has an obvious mode-3 structure, and is weaker in am-

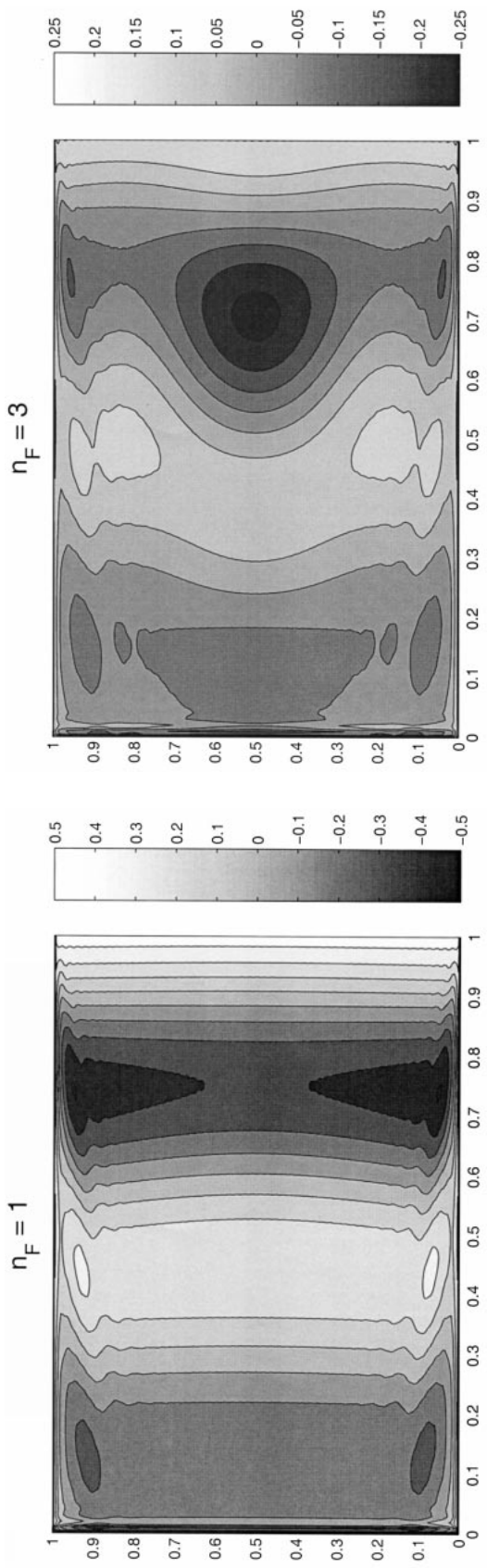

FIG. 10. Snapshots of the streamfunction from the 2D solution with $\omega = 1 \times 10^{-3}$, $r = 1 \times 10^{-4}$, $k = 0$, and $\lambda = 0.01$; the upper solution results from forcing with a meridional wavenumber of one, and the lower with a wavenumber of two.

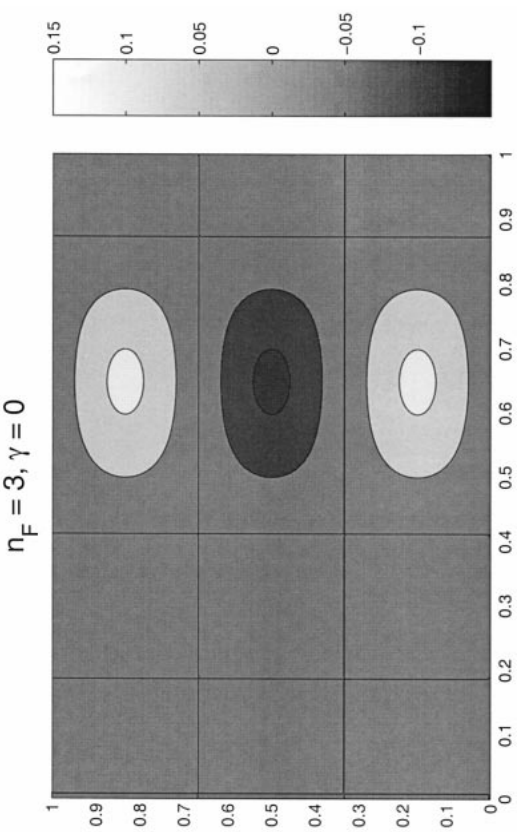

FIG. 11. The streamfunctions for forcing at a meridional wavenumber of three. The upper panel shows the solution in which $\psi = \Gamma(t)$ on the boundary, and the lower shows the solution with $\psi = 0$ on the boundary. The other solution parameters are as in the previous figure.

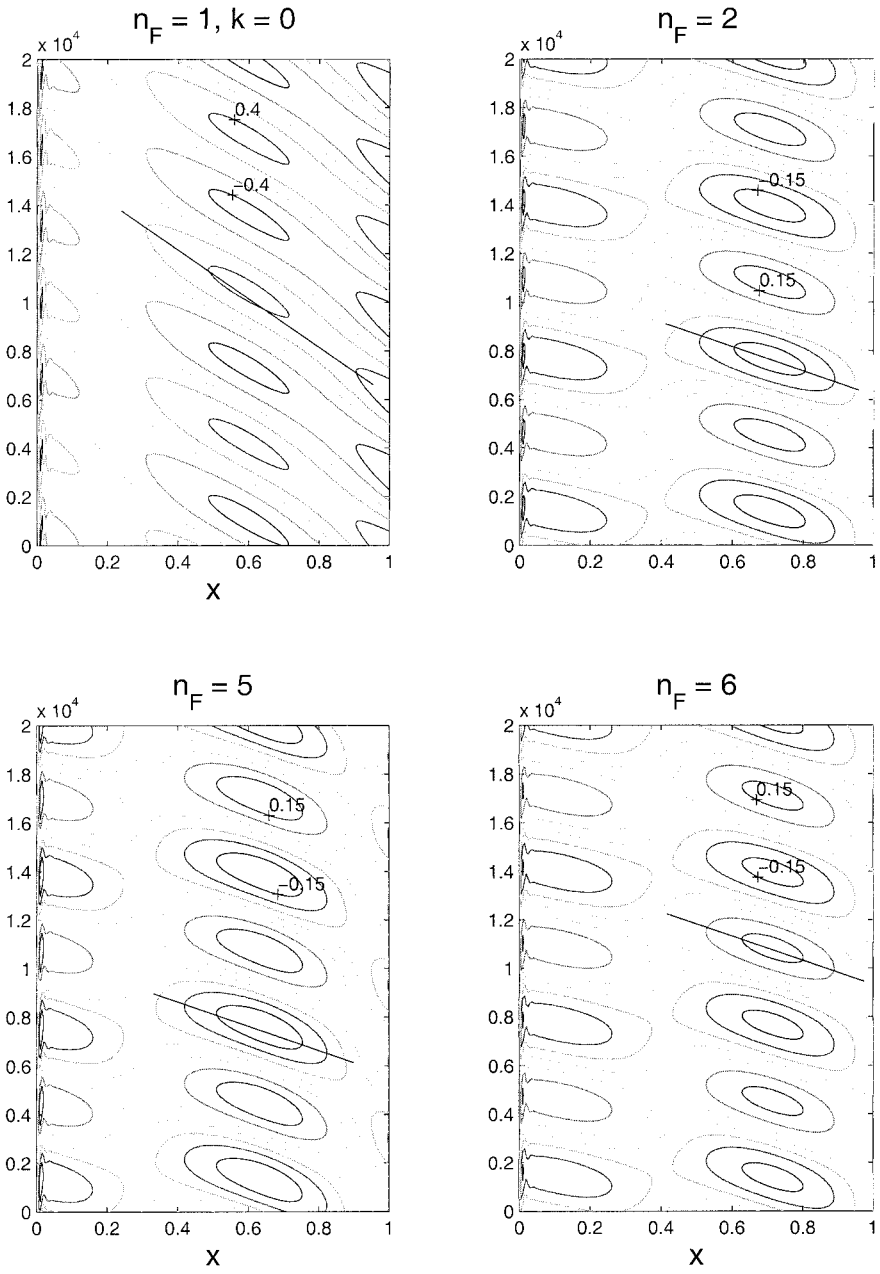

FIG. 12. Time–longitude plots with different meridional forcing scales. The parameters are $\omega = 1 \times 10^{-3}$, $r = 1 \times 10^{-4}$, $k = 0$, and $\lambda = 0.01$. The solid line in the upper-left panels represents the long-wave phase speed, and the other lines represent the augmented phase speed, c_l. The contour values are (upper left) $\pm$[0.2.4] and (upper right and lower panels) $\pm$[0.05.1.15]. Notice the tendency for decreasing amplitude with increasing wavenumber.

plitude. The wave crests change sign as they pass the basin center, but remain confined to their respective one-third basins. The speed of westward propagation is greater than that in the upper panel.

The differences in phase speed are seen clearly in the time–longitude plots (Fig. 12). Here, $\omega = 0.1\lambda$, $r = 0.01\lambda$, and again $y = 1/(2n_F)$ and $k = 0$. With $n_F = 1$, the long-wave phase speed is evident (upper left panel), but in the other cases we observe the augmented phase speed, which is $c_l = -2\lambda^2$ for $k = 0$. The reason, as noted above, is the superposition of the long and the directly forced waves. With still larger values of n_F, the directly forced wave is the strongest (not shown).

The shift in apparent phase speed with increasing zonal and meridional wavenumbers is tabulated in Fig. 13. The phase speeds from various solutions were mea-

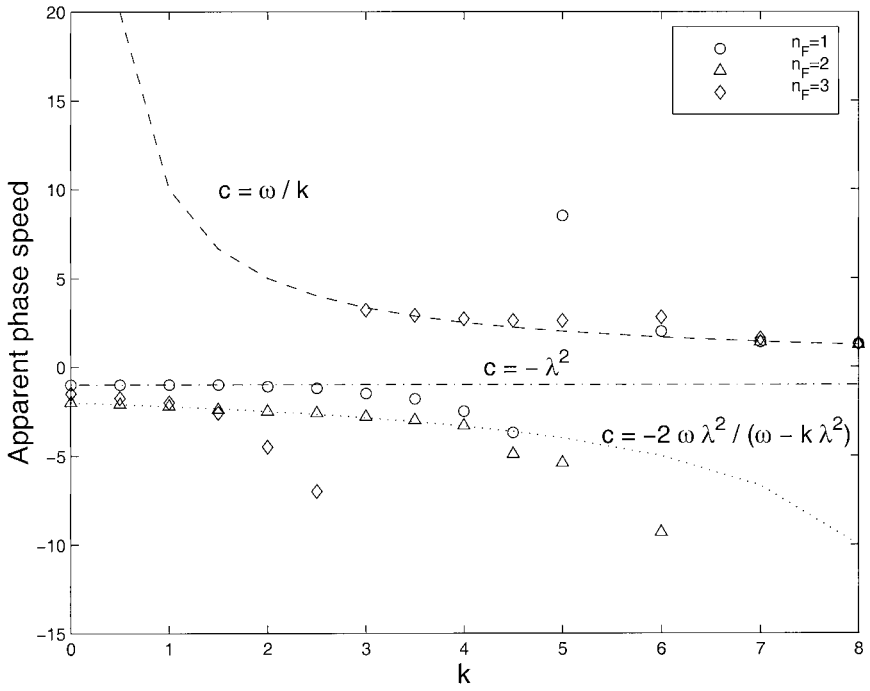

FIG. 13. Empirically derived phase speeds with three different values of the meridional wavenumber, n_F. The dashed line indicates the wind phase speed, the dash–dot line the long Rossby wave speed, and the dotted line the augmented phase speed, c_l.

sured by drawing a line through a representative wave crest. With $n_F = 1$ (circles), the phase speed is the long-wave speed at the gravest zonal wavenumbers. But increasing k causes the apparent speed to increase in the westward direction. Eventually it undergoes a transition to the (eastward) wind phase speed (the dashed line) because the directly forced wave dominates. Defining the apparent speeds in the transition region is somewhat subjective, but they are clear in the high and low k limits.

With $n_F = 2$, the phase speeds at the gravest zonal wavenumbers are instead the augmented phase speed, c_l (the dotted line) because $\psi = 0$ on the boundary. But increasing k likewise causes a transition to the wind phase speed. With $n_F = 3$, the speed is near the long-wave speed for small k, but makes the transition to the wind speed earlier because the combination of smaller zonal and meridional forcing scales favors the directly forced response.

Consistent with the above statements, the directly forced wave dominates at all k with much larger values of n_F. As such, the phase speeds fall around the dashed line, and the phase speed at $k = 0$ is infinite.

One can speculate about the response to forcing with a spectrum of forcing frequencies and scales. We have seen that the most energetic response is at the largest forcing scales, and, presuming the difference between meridionally asymmetric and symmetric forcing does not hold beyond QG, this means the long wave speed will be observed. However, the strength of the response does not decrease fast enough with forcing wavenumber to rule out observing augmented speeds, so a mix of apparent speeds is probably to be expected (see also below).

7. Boundary forcing

It is thought that coastal Kelvin waves radiate Rossby waves into the interior of the Pacific (e.g., Cox 1987), and this is presumedly a very different driving mechanism than wind forcing. In the present context, this is the response to the boundary oscillation itself, that is, $\Gamma(t)$, in the absence of the wind. Such a solution is easily obtained from (9). Though mass is no longer conserved if the amplitude of the boundary oscillation is specified, the solution is nonetheless instructive.

The equation for the basin response to boundary driving is like that in (2), except that $F = 0$ and the streamfunction is normalized using the amplitude of the prescribed boundary oscillation. Moreover there is no y variation, so the solution is obtained in the same manner as for (9) and differs from (9) only in that $\gamma = 1$ and $1/N = 0$. The boundary driven solution has only the westward propagating wave terms because the directly forced wave is now gone. The frequency and dissipation dependence of the two westward waves is exactly as described in section 4a; for example, they are trapped in unequal boundary layers at low frequencies, with the long wave extending farther into the interior, and trapped in deformation-scale boundary layers when $\omega > \lambda/2$. The solution is easier to characterize than the

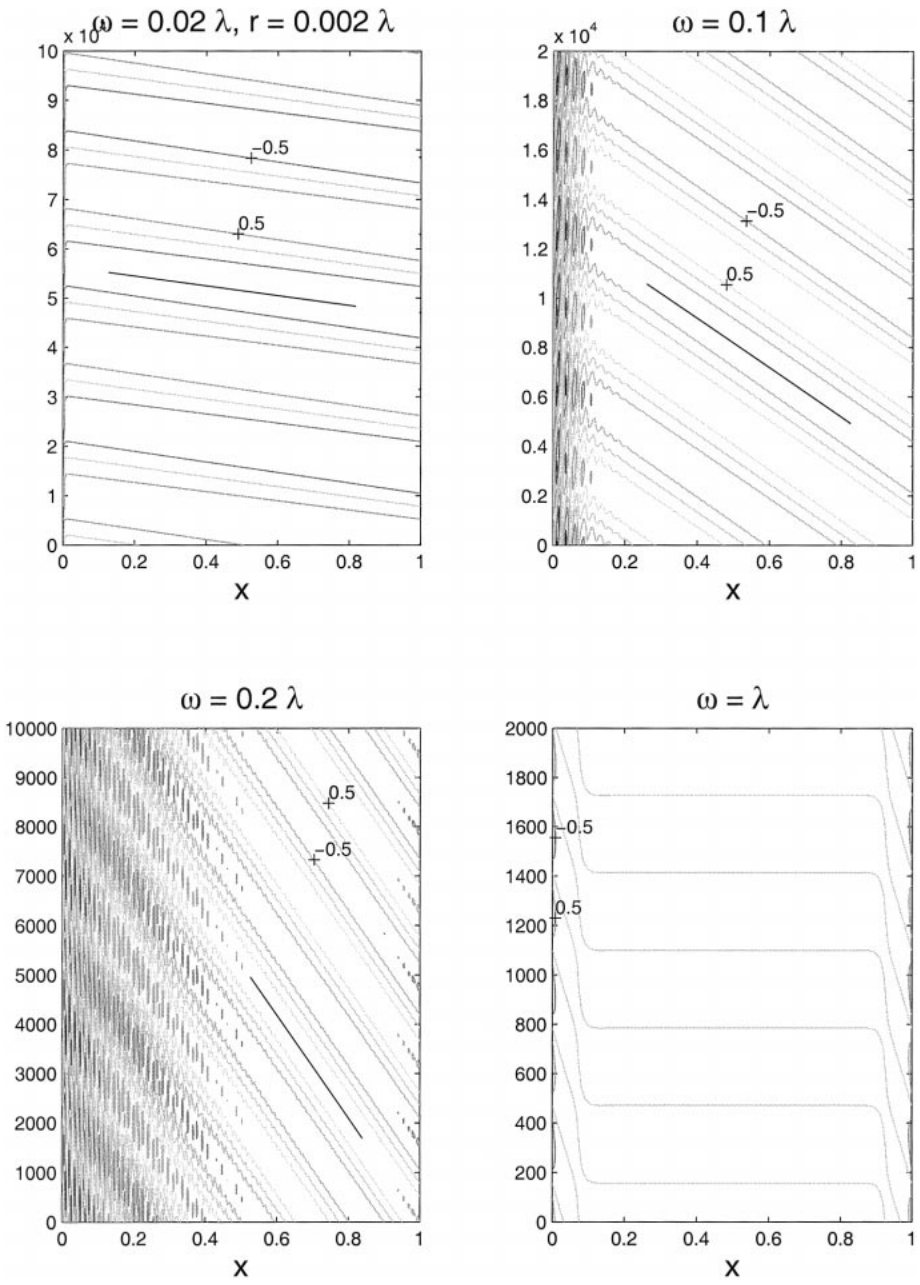

FIG. 14. Time–longitude plots of basin waves driven by a boundary oscillation with a fixed amplitude, i.e. $\Gamma = \exp(-i\omega t)$. The parameters are the same as in Fig. 4. The solid lines in the upper panels correspond to $c = -\lambda^2$, and to $c = -0.95\lambda^2$ in the lower left panel. The contour values are $\pm[0.511.5]$.

wind-forced one because there is no k (nor n_F) to worry about.

The time–longitude plots of the solution with parameters like those in Fig. 4 are shown in Fig. 14. A similar frequency dependence is evident; however, the phase speed, without the directly forced wave, is always clearly that of the long wave (so long as $\omega < \lambda/2$). As in Fig. 4, the phase speed is about 5% slower in the $\omega = 0.2\lambda$ case but, in general, boundary forcing is much more likely to yield phase propagation at (or near) the long-wave speed.

8. Summary

Wind-forced, baroclinic Rossby waves in a basin comprise three wave constituents: a directly forced wave (which tracks the wind), and a short and a long wave with westward phase speeds. The apparent phase speed

depends on which constituents are present in the interior and on their relative amplitudes. With a low forcing frequency and at least some dissipation, the long wave and the directly forced are dominant in the interior.

Perhaps the most important result is that the character of the solution depends strongly on the boundary condition. Demanding that $\psi = 0$ there, which yields a solution that does not conserve mass (McWilliams 1977; Flierl 1977), forces the long and directly forced waves to have the same amplitude. With $\psi = \Gamma(t)$ on the boundary, a mass-conserving solution is found and the long Rossby wave can be much the strongest constituent. The change in boundary condition also alters the basin resonances by permitting communication from the western to the eastern wall without short Rossby waves; the resulting waves have a different dispersion relation and are much less susceptible to damping than the traditional basin modes.

The long Rossby wave dominates at low frequencies when the interface moves significantly at the boundary. This occurs when the forcing possesses large meridional and zonal scales. And when the long wave dominates, the observed phase speed is the long-wave speed. Smaller interfacial deflections obtain with lesser forcing scales, and the long wave is weaker. Then one may observe augmented phase speeds due to the superposition with a comparably strong directly forced wave (as occurs in the long-wave solution of White 1977; section 3). The same is true when the forcing is antisymmetric about the basin's middle latitude because then $\psi = 0$ on the boundaries; however this may well be an artifact of the QG approximation, which demands the interfacial displacement be uniform around the entire boundary.

At frequencies larger than the maximum free wave frequency, $\lambda/2$, the two westward waves are trapped in deformation-scale boundary layers and the interior response is weak. At intermediate frequencies, both westward waves are present in the interior; one observes substantial small-scale structure superimposed on a signal propagating near the long-wave speed.

Lastly, with boundary forcing there is no directly forced wave in the interior and the long westward wave determines the phase speed. As such, the speed is approximately the long-wave speed, as long as $\omega < \lambda/2$.

9. Discussion

As noted, the cutoff frequency, above which the interior response is weak, is $\omega = \lambda/2$. This corresponds to a period, which can be written (dimensionally) as

$$T_c = \frac{2\pi}{\beta L}\left(\frac{2L}{L_R}\right) = \frac{4\pi}{\beta L_R},$$

where L_R is the Rossby radius. With $L_R = 30$ km, the cutoff period T_c is about 7.2 months at 10°N and 9.2 months at 40°N (the discrepancy with the previous results comes from the fact that $\lambda \approx 0.0033$ in the Pacific). Only forcing with greater periods can produce westward phase propagation.

Though the present system is very simple, the results may pertain to the findings of Chelton and Schlax (1996). The authors observe phase speeds consistent with the long Rossby wave speed in the Tropics, but larger phase speeds in the subtropics. We know that boundary forcing is important at low latitudes, and less important in the subtropics (Chelton and Schlax 1996; Qiu et al. 1997) where it is believed that wind forcing is a more important driving mechanism (White and Saur 1981). Given the present results, the long-wave speed should be prevalent when boundary forcing is dominant (the same point is suggested by Qiu et al. 1997). With wind forcing, the long-wave speed is still possible, but so too are faster phase speeds, and even eastward propagation.

The results also agree broadly with the findings of Zang and Wunsch (1999). Their data suggests that large zonal wavenumbers exhibit the long-wave speed at midlatitudes but that phase speeds increase with larger wavenumbers. This is qualitatively consistent with Fig. 13. They also find instances of infinite phase speeds with $k = 0$. As noted above, if n_F is large enough, an infinite phase speed is expected because that is the phase speed of the wind with $k = 0$. The agreement between the present results and theirs may be fortuitous, but this explanation is appealing, at least for its simplicity; that is, one need not invoke topography, a mean flow, or nonlinear effects.

As discussed above, it is the superposition of the forced and long waves that is responsible for augmented phase speeds here, as was also the case in White (1977). But, because White used the $\psi = 0$ boundary condition, augmented phase speeds were found over the entire range of forcing frequencies. It is important to note that, if the method of processing the altimeter data is capable of distinguishing the directly forced and free components (and the amount of data great enough), the present results suggest the free components ought to have speeds at or near the long-wave speed, and the augmented phase speeds would no longer obtain. If they do, one would have to invoke other explanations such as surface trapping (e.g., Samelson 1992).

As stated, the quasigeostrophic equations, with a constant value of β and small interfacial displacements, are probably inappropriate for basin-scale motion. A better set might be the planetary geostrophic equations, which permit order-one interfacial deviations (i.e., outcropping) as well as a meridionally variable β. Such equations also open the possibility for wave steepening (Charney and Flierl 1981) but exclude relative vorticity so that a western boundary is not possible without higher order dynamics.

Nevertheless, it is of some interest to see how the present results would change with such a system. Of primary interest is how the resonances change (section

5) when Kelvin waves have a finite velocity, or even if they exist at all. And the dependence on meridional variations in the forcing seen here (including the meridional symmetry issue) may well vary when both β and the layer depth also have large-scale variations. Shallow water numerical studies suggest that a quasigeostrophic model employing the conservation of mass condition mimics well the adjustment of a primitive equation basin (Milliff and McWilliams 1994), but more work is required to discover to what extent the waves change.

Acknowledgments. The work was supported in part by the Charles Davis Hollister Fund and the Penzance Endowed Fund for assistant scientist support at WHOI. The comments of Joe Pedlosky were very valuable, particularly with regards to the boundary conditions and to basin resonances. I found out after submitting the paper that Paola Cessi, too, had been studying the change in basin waves upon altering the boundary condition, and we discussed that. I also enjoyed several conversations with Carl Wunsch, Breck Owens, and Ken Brink.

REFERENCES

Charney, J. G., and G. R. Flierl, 1981: Oceanic analogues of large-scale atmospheric motions. *Evolution of Physical Oceanography,* B. A. Warren and C. Wunsch, Eds., The MIT Press, 504–548.

Chelton, D. B., and M. G. Schlax, 1996: Global observations of oceanic Rossby waves. *Science,* **272,** 234–238.

Cox, M., 1987: An eddy-resolving numerical model of the ventilated thermocline: Time dependence. *J. Phys. Oceanogr.,* **17,** 1044–1056.

de Szoeke, R. A., and D. B. Chelton, 1999: The modification of long planetary waves by homogeneous potential vorticity layers. *J. Phys. Oceanogr.,* **29,** 500–511.

Dewar, W. K., 1998: On ''too fast'' baroclinic planetary waves in the general circulation. *J. Phys. Oceanogr.,* **28,** 1739–1758.

Flierl, G. R., 1977: Simple applications of McWilliams' ''A note on a consistent quasigeostrophic model in a multiply connected domain.'' *Dyn. Atmos. Oceans,* **1,** 443–453.

Gill, A. E., 1982: *Atmosphere–Ocean Dynamics.* Academic Press, 662 pp.

Killworth, P. D., D. B. Chelton, and R. A. de Szoeke, 1997: The speed of observed and theoretical long extratropical planetary waves. *J. Phys. Oceanogr.,* **27,** 1946–1966.

McWilliams, J. C., 1977: A note on a consistent quasigeostrophic model in a multiply connected domain. *Dyn. Atmos. Oceans,* **1,** 427–441.

Milliff, R. F., and J. C. McWilliams, 1994: The evolution of boundary pressure in ocean basins. *J. Phys. Oceanogr.,* **24,** 1317–1338.

Pedlosky, J., 1965: A study of the time dependent ocean circulation. *J. Atmos. Sci.,* **22,** 267–272.

——, 1987: *Geophysical Fluid Dynamics.* Springer-Verlag, 710 pp.

Qiu, B., W. Miao, and P. Muller, 1997: Propagation and decay of forced and free baroclinic Rossby waves in off-equatorial oceans. *J. Phys. Oceanogr.,* **27,** 2405–2417.

Rhines, P. B., 1970: Edge-, bottom- and Rossby waves in a rotating, stratified fluid. *Geophys. Fluid Dyn.,* **1,** 273–302.

Samelson, R. M., 1992: Surface-intensified Rossby waves over rough topography. *J. Mar. Res.,* **50,** 367–384.

White, W. B., 1977: Annual forcing of baroclinic long waves in the tropical North Pacific. *J. Phys. Oceanogr.,* **7,** 50–61.

——, and J. F. T. Saur, 1981: A source of annual baroclinic waves in the eastern subtropical North Pacific. *J. Phys. Oceanogr.,* **11,** 1452–1462.

Zang, X., and C. Wunsch, 1999: The observed dispersion relationship for North Pacific Rossby wave motions. *J. Phys. Oceanogr.,* **29,** 2183–2190.